Appl Phys B (2009) 94: 411–427
DOI 10.1007/s00340-008-3287-9

Applied Physics B
Lasers and Optics

Thermal effects in singly resonant continuous-wave optical parametric oscillators

M. Vainio · J. Peltola · S. Persijn · F.J.M. Harren · L. Halonen

Received: 25 August 2008 / Revised version: 15 October 2008 / Published online: 15 November 2008

Abstract Stability and tuning characteristics of continuous-wave optical parametric oscillators (CW OPOs) are affected by various thermal effects arising from optical absorption in nonlinear crystals. In this paper, we present an experimental study of such effects in a singly resonant CW OPO. The OPO operates in the 3-μm mid-infrared region and it is based on a MgO-doped periodically poled lithium niobate crystal. We focus our study on two thermally induced phenomena that have been recently reported to exist in singly resonant CW OPOs: optical bi-stability and thermal self-locking. Thermal self-locking effect, which is known to alter the stability and tuning properties of doubly and triply resonant CW OPOs, is shown to be also of importance in singly resonant OPOs. We report the stability and tuning characteristics of a thermally loaded OPO and discuss a simple temperature-tuning method that can be used to scan the OPO idler frequency continuously over several THz.

PACS 42.65.Yj · 42.72.Ai

M. Vainio · J. Peltola · L. Halonen (✉)
Laboratory of Physical Chemistry, University of Helsinki,
P.O. Box 55, A.I. Virtasen aukio 1, 00014 Helsinki, Finland
e-mail: lauri.halonen@helsinki.fi

S. Persijn
Nederlands Meetinstituut, Thijsseweg 11, 2629 JA Delft,
The Netherlands

F.J.M. Harren
Life Science Trace Gas Facility, Molecular and Laser Physics,
Institute for Molecules and Materials, Radboud University,
P.O. Box 9010, 6500 GL Nijmegen, The Netherlands

1 Introduction

Single-frequency, continuous-wave optical parametric oscillators (CW OPOs) are excellent coherent light sources for applications that require a combination of high spectral resolution and large wavelength tuning. This includes various applications of optical radiometry [1] and molecular spectroscopy, such as trace gas detection [2, 3] and frequency metrology [4, 5]. The CW OPOs are most commonly used in wavelength regions where the availability of other laser sources is limited, in particular, in the mid-infrared region above 2 μm. While doubly and triply resonant OPOs can be operated with low-power (1 to 100 mW) pump lasers, the highest output power (several watts) and the most convenient wavelength tuning can be obtained using singly resonant optical parametric oscillators, SROs [3, 6–11]. In its simplest configuration, a single-mode, tunable SRO consists of a pump laser and of an optical cavity containing the nonlinear material [6, 10, 11]. Often, an intra-cavity etalon is included for improved single-mode operation and/or for frequency tuning [3, 6–9].

Although the SROs can be structurally very simple, their operation is in practise complicated by residual etalon effects and by photorefractive and thermal effects in the nonlinear crystal. Thermal effects arise from the absorption of optical power in the crystal, which leads to a temperature gradient within the beam volume. Usually, the most important thermal effects are thermal lensing and de-phasing, but also spectral instabilities can occur. In the mid-infrared (MIR) OPOs, the crystal heating is most often due to high absorption at the idler wavelength [12, 13] or due to absorption of large intra-cavity signal power [14]. Idler absorption is particularly important at wavelengths longer than 4 μm. The effect of large idler absorption on the OPO threshold and power has been previously studied both theoretically

[12] and experimentally [13, 15]. Here we discuss a SRO that operates at around 3-μm idler wavelength and is made resonant at the signal wavelength. In a typical high-finesse resonance cavity, the intra-cavity signal power can excess 1 kW [14], while the pump and idler powers are two orders of magnitude smaller.[1] An efficient way of reducing thermal load in the nonlinear crystal is hence to reduce the intra-cavity signal power, for example, by using an output coupler that partly transmits the signal. The use of a partly transmitting output coupler has been demonstrated with CW OPOs already in the 1990s [6]. It has been studied more carefully only recently [9, 14] as high power single-frequency pump lasers and better nonlinear materials have become commercially available. Previously, the cavities of SROs were often designed for the highest possible finesse at the signal wavelength, in order to keep the oscillation threshold as low as possible (typically 1–4 W in the MIR SROs). This was necessary as the single-frequency pump laser output powers were limited to below 10 W. It should be noted that, even if the threshold is increased, the use of an output coupler does not necessarily reduce the attainable idler power. In fact, the single-frequency output power can be higher than in the case of a high-finesse cavity [9, 11, 14]. This is because the spectral instabilities (multi-mode operation, Raman lasing) related to high intra-cavity intensities can be better avoided. In addition, high signal powers of several watts, compared to ∼100 mW, can be extracted by replacing one of the highly reflecting cavity mirrors with an output coupler.

Partly because of the thermal effects, the difficulties of obtaining large continuous wavelength tuning and good long-term stability have prevented a widespread use of the SROs. Trace gas detection is an example of a spectroscopic application that requires large and continuous tuning range. The measurements are typically done in atmospheric pressure, which means that the molecular absorption lines are several GHz wide. In order to reliably address a line and in order to perform multi-gas analysis, continuous tuning range of hundreds of GHz is needed. One way of performing mode-hop-free scanning is to scan the OPO cavity length synchronously with an intra-cavity etalon [17, 18]. The advantage of this technique is that both the signal and idler frequencies can be continuously scanned without mode hops. However, the technique is limited by etalon walk-off losses and by photorefractive and thermal effects in the nonlinear crystal, and the largest mode-hop-free tuning range reported so far is 38 GHz [17]. Much larger idler tuning range can be obtained by using the OPO as a passive pump-to-idler frequency converter, in which the signal frequency is fixed and the pump frequency tuning is directly converted into idler tuning. Mode-hop-free idler tuning of more than 100 GHz has been demonstrated with the modern pump lasers [7, 10, 11].

Mode-hop-free operation of over several hours is needed in real-time trace gas analysis and in certain applications in metrology and quantum optics [17]. In most cases the stability of the OPO frequency can be improved by locking it to an external reference. An example of this is a pump-resonant SRO, in which the cavity length was locked to a stable pump laser, providing a highly stable mode-hop-free operation for 58 h [19]. Even when stabilising the OPO to an external reference, good passive stability is required for reliable long-term operation. To keep the setup simple and to allow for convenient frequency tuning, it would be desirable to have an OPO that has such a good passive stability that locking to an external frequency reference is not necessary. So far, only two demonstrations of a mode-hop-free, long-term stable, purely singly resonant OPO have been reported: In the first one, idler frequency drift of less than 400 MHz over 30 h was obtained using a temperature stabilised SRO [20]. Recently, we have reported a signal frequency drift of $<$150 MHz and idler power drift of $<$1.2% over a period of 20 h with a simple two-mirror SRO [11]. Our SRO differs from the previously demonstrated devices in that it needs no intra-cavity etalon for reliable long-term single-mode operation. Stable operation is obtained by careful control of the crystal temperature and thermal effects.

In this paper, we extend our previous work by presenting a detailed study of thermal effects in a singly resonant MIR OPO. In Sect. 2, we describe the experimental setup and prepare the discussion on thermal effects by investigating the absorption of Mg-doped lithium niobate, which is the most commonly used optical nonlinear material in the MIR OPOs. In Sect. 3, we report and analyse the experimental results. This includes the first observation of optical bi-stability in a SRO that resonates the signal frequency. Bi-stability is attributed to thermal lensing and to axial mismatch between the pump and signal beams. We discuss the spectral purity of a thermally loaded SRO and describe the conditions needed to obtain stable single-mode operation. We have observed that the stability and frequency tuning properties of the OPO are affected by a thermal self-locking effect, even if the OPO intra-cavity power was limited by using a partly transmitting output coupler mirror. Thermal locking is analysed in Sect. 3, and the stability and tuning characteristics of the OPO are reported in Sect. 4.

2 Experimental setup

The experimental setup used in this work is schematically shown in Fig. 1. The setup consists of a singly resonant CW OPO and of instrumentation used to study the OPO characteristics. The OPO produces watt-level CW output in

[1] A SRO resonant at the idler has also been demonstrated [16]. In that case the thermal load is, naturally, dominated by idler absorption.

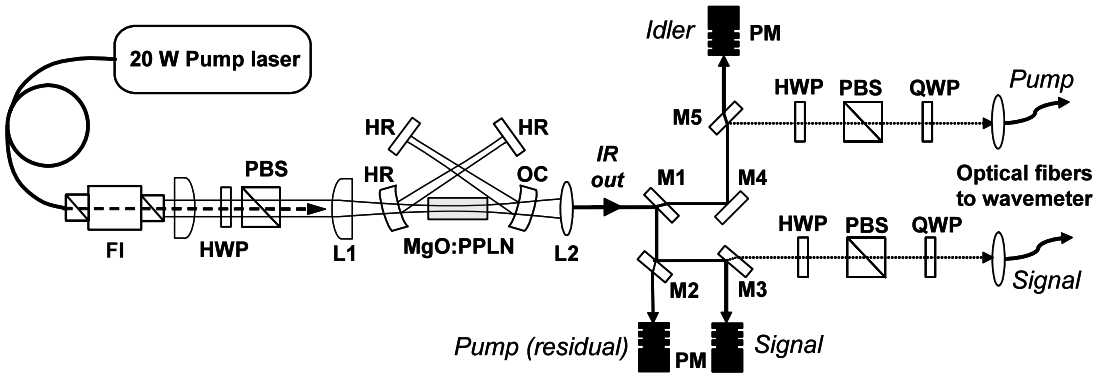

Fig. 1 Schematics of the experimental setup. The pump laser light is coupled into the OPO cavity through a Faraday isolator (FI) and a focusing lens L1. A combination of a half-wave plate (HWP) and a polarising beam splitter (PBS) is used to control the pump power incident to the OPO. The cavity consists of three highly reflective (HR) mirrors and an output coupler (OC) that transmits ∼2% of the signal beam. Output beams are collimated using an uncoated CaF_2 lens L2. Idler beam is separated from the residual pump beam using two dichroic mirrors (M1 and M5) and a gold mirror M4. Signal beam is separated from the pump using dichroic mirrors M2 and M3. Small fractions of the pump and signal beams are directed to a wavemeter using optical fibres. The power level incident to a fibre coupler is controlled using a half-wave plate and a polarising beam splitter. Quarter-wave plates (QWP) are included in order to block the back reflections from the fibre couplers. Three alternative positions of the optical power meter (PM) are shown

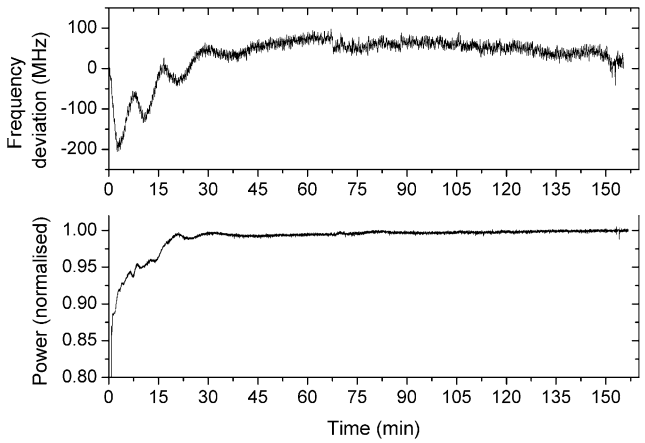

Fig. 2 Measured frequency and power stability of the pump laser (IPG YLR-20-1064-LP-SF). Measurement was started right after turning the laser on, and a sampling interval of 1 s was used. Laser output power was set to 10 W

the mid-infrared idler region 2.7–3.45 μm and in the near-infrared signal region 1.54–1.76 μm. The OPO is pumped with a narrow-linewidth (70 kHz), polarisation maintaining fibre laser (IPG YLR-20-1064-LP-SF). The laser has an integrated fibre amplifier that can provide a maximum output power of 20 W. Laser wavelength is 1064 nm and it can be continuously tuned over 140 GHz by changing the laser temperature. A Faraday isolator is used at the laser output to prevent back-reflections from the OPO setup. The laser reaches the maximum frequency and power stability after a warm-up period of 45 to 60 min (Fig. 2). After the warm-up, the laser typically stabilises in a few minutes after changing the power setting. If faster stabilisation is needed, a combination of a half-wave plate and a polarising beam splitter can be used to vary the OPO pump power without disturbing the laser.

The pump laser beam is focused into the nonlinear crystal using a plano-convex lens, which is anti-reflection coated for the pump wavelength. Pump laser focusing parameter can be varied by using lenses with different focal lengths; tight focusing into the crystal is possible due to the large beam diameter (4 mm) of the collimated laser output. The nonlinear material is a 5-cm long and 1-mm thick congruent MgO:PPLN, i.e. a periodically poled lithium niobate crystal, which is MgO-doped. Doping level is 5 mol%, which significantly improves resistance against photorefractive damage [21, 22]. The crystal is manufactured by HC Photonics (Taiwan) and it has seven separate poling periods, ranging from 28.5 to 31.5 μm. Both surfaces of the crystal are angle-polished (1°) and anti-reflection (AR) coated for the three OPO wavelengths in order to avoid parasitic etalons inside the OPO cavity. Residual power reflectivities stated by the manufacturer are <1 and $<0.75\%$ at the pump and signal wavelengths, respectively. Temperature of the crystal is controlled using thermo-electric coolers (Peltier-elements) and a commercial controller (Newport 350B). With our current setup the temperature can be stabilised to within ±6 mK anywhere between 20 and 120°C. The crystal mount is covered with Teflon in order to improve thermal isolation and to protect against air currents.

We have used both two-mirror and four-mirror OPO cavity designs [11]. The measurements reported in this paper have been mostly done using the four-mirror design shown in Fig. 1, because it is well-suited for exploring the OPO behaviour with different parameter combinations. Compared to the two-mirror cavity, the four-mirror cavity gives more degrees of freedom for cavity design and allows for smaller

waist size in the middle of the crystal. The four-mirror cavity can be used both in linear (standing wave) and ring configurations [6]. Most of the singly resonant OPOs reported so far are based on the ring cavity, which is commonly considered to have superior stability properties compared to the linear cavity. We have observed that, if the residual optical reflections inside and outside of the cavity are carefully suppressed and if the nonlinear crystal is properly temperature stabilised, the linear cavity can provide stability and tuning properties comparable to those of the ring cavity. In practise, the linear cavity can provide even enhanced operation over the ring cavity, because the linear cavity is easier to align and because it is less sensitive to small misalignments.

In the standard configuration, all the cavity mirrors are highly reflective at the signal wavelength ($R > 99.9\%$ @ 1550–1750 nm) and highly transmitting at the pump and idler wavelengths ($R < 0.5\%$). However, in order to decrease thermal load in the crystal, we have used an output coupler with smaller signal reflectivity. The output coupler reflectivity is 98% at a signal wavelength of 1650 nm (corresponding to idler wavelength $\lambda_\mathrm{i} = 3000$ nm) and varies between 97 and 98.5% over the signal tuning range. Rear surfaces of the mirror substrates are anti-reflection coated for all three wavelengths in order to minimise optical feedback from them. This was thought to be necessary as the curved mirrors are of convex/concave type and any reflections from their rear surfaces would overlap with the cavity mode. The same applies to the plane mirrors that have parallel substrate surfaces. The anti-reflection (AR) coatings are not as important in the ring configuration, in which the reflections from back of the substrates are laterally shifted with respect to the cavity mode. In addition to minimising the intra-cavity etalon effects, we have also avoided direct optical feedback from outside of the cavity by slightly tilting the pump focusing lens and the output collimating lens relative to the optical axis.

2.1 Cavity design

The efficiency of parametric conversion can be optimised by selecting the pump and signal focusing parameters so that they are (nearly) equal to each other and within the range $\xi = 1, \ldots, 7$ [23, 24]. (The focusing parameter is defined as $\xi = L_\mathrm{c}/b$, where L_c is the crystal length and $b = 2\pi {w_\mathrm{x}}^2/\lambda$ is the confocal parameter of the Gaussian beam. The parameter w_x is the beam waist ($1/\mathrm{e}^2$-intensity radius) and λ is the wavelength.) The starting point for the cavity design process is to select a waist size that maximises the parametric conversion efficiency, and to select cavity dimensions that produce the desired waist. The desired waist size of the pump beam is determined by the initial beam parameters and by the lens(es) used to focus the beam into the nonlinear crystal. Both the pump and signal waists can be calculated using the ABCD-matrix method for a Gaussian beam. The method is discussed in most textbooks on laser optics. We briefly recall this procedure for the OPO cavity, so that we can later refer to it when discussing how thermal lensing alters the OPO compared to its cold-cavity operation.

If we use a symmetric cavity and place the beam waist in the middle of the crystal, it is sufficient to study just one half of the cavity in order to calculate its dimensions. The signal beam waist size $w_{1\mathrm{s}}$ between the concave mirrors of a four-mirror cavity, see the inset of Fig. 3, is given by [25]

$$w_{1\mathrm{s}} = \left[\frac{\lambda_\mathrm{s}^2}{\pi^2}\left(f^2\frac{d_1 - f}{d_2 - f} - (d_1 - f)^2\right)\right]^{1/4}, \tag{1}$$

where f is the focal length of the concave mirrors ($f = ROC/2 = 50$ mm). The distance between the primary waist $w_{1\mathrm{s}}$ and a concave mirror is denoted by d_1. A cavity leg is closed by a secondary waist $w_{2\mathrm{s}}$, which is separated by a distance d_2 from the concave mirror. In the ring cavity, the secondary waist is located between the two plane mirrors, and in the linear cavity it is on a plane mirror. The distances used in (1) are optical distances. The distance d_1 can be converted into a physical cavity dimension by taking into account the crystal refractive index n_s seen by the signal beam:

$$d_{1\mathrm{Phys}} = d_1 + \frac{L_\mathrm{c}}{2}\left(1 - \frac{1}{n_\mathrm{s}}\right). \tag{2}$$

To ensure small sensitivity of the beam waist size to changes of the cavity dimensions, the dimensions are often selected so that they correspond to the centre of the cavity stability region. In Fig. 3 we have plotted the waist size vs. cavity dimensions for a cavity used in our previous work [11]. The same cavity is used in this work, if not stated otherwise. The cavity was designed to provide a signal focusing parameter of $\xi_\mathrm{s} = 2$, which at a wavelength of 1611 nm corresponds to a waist size of 55 µm. With the given concave mirrors ($f = 50$ mm), the total optical length of the cavity is 0.7 m. In the case of a linear cavity this gives a longitudinal mode spacing of $FSR = 210$ MHz.

In four-mirror cavities the signal beam enters the concave mirrors in an angle different from normal incidence, which introduces astigmatism [25, 26]. The effective radius of curvature of the mirror depends on the angle of incidence θ and is given by $R_\mathrm{sag} = R/\cos\theta$ and $R_\mathrm{tan} = R\cos\theta$ for the sagittal and tangential planes, respectively [25]. This leads to different waist sizes in the two planes, $w_{1\mathrm{sag}}$ and $w_{1\mathrm{tan}}$. In our case, the mechanical structure of the crystal mount is such that the minimum angle of incidence that can be used is about 16 degrees. The resulting effect on the beam waist size is plotted in Fig. 3. At the cavity design point, the astigmatism defined as $(w_{1\mathrm{sag}} - w_{1\mathrm{tan}})/w_{1\mathrm{sag}}$ is ∼10%. The maximum deviation from the non-astigmatic value is −15% with the cavity configurations considered here. This deviation was considered to be small and we constructed the cavities according to the calculations that do not take astigmatism into account.

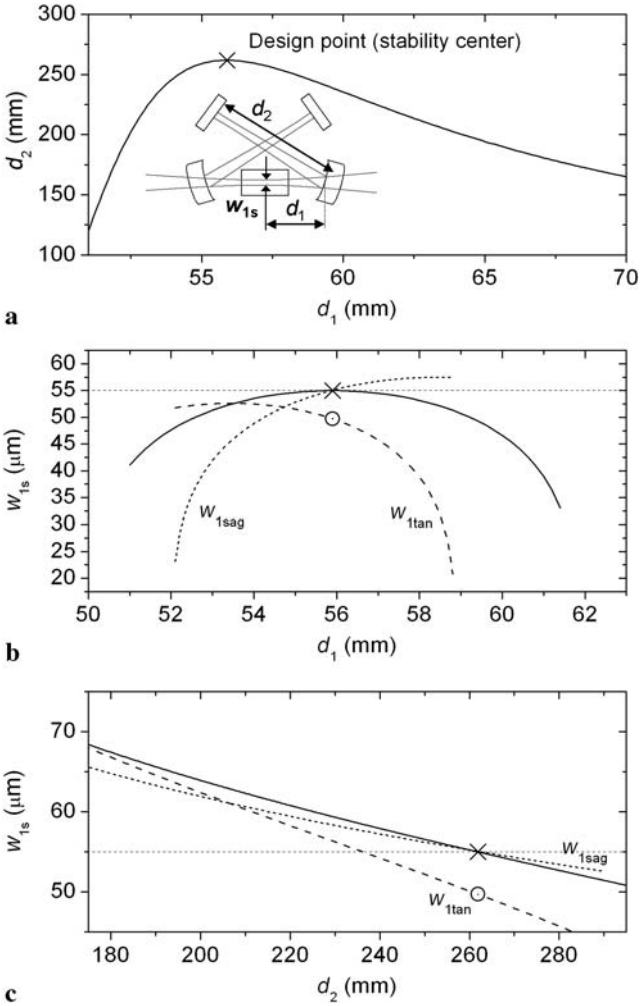

Fig. 3 Calculated dimensions of the four-mirror OPO cavity that is designed to provide a signal focusing parameter of $\xi_s = 2$. At a wavelength of 1611 nm, the design waist size in the middle of the MgO:PPLN crystal is $w_{1s} = 55$ μm, which is obtained with $d_1 = 55.9$ mm and $d_2 = 262$ mm. This point is marked with crosses in the figures. **b** and **c** show the change of waist size as a function of cavity dimensions d_1 and d_2, respectively. The solid curve represents the ideal case without astigmatism, and the dashed curves show the effect of astigmatism caused by 16° incident angle of the signal beam on the curved mirrors. Abbreviations "sag" and "tan" refer to the waist sizes in the sagittal and tangential planes, respectively

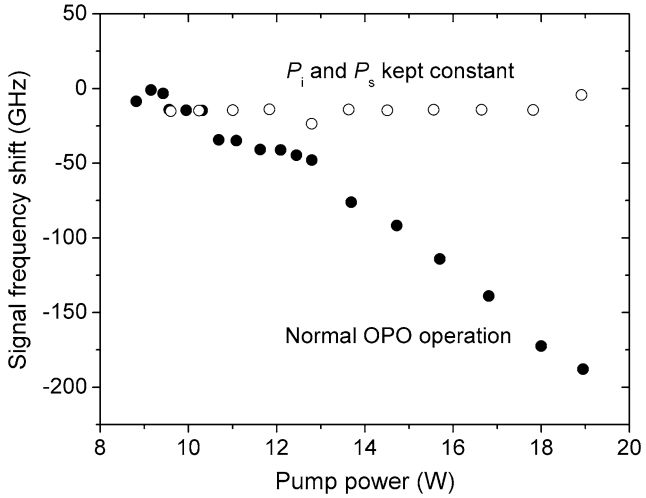

Fig. 4 Thermally induced frequency shift versus pump power. In the normal operation the entire pump power directed into the crystal is e-polarised, which leads to crystal heating due to the increased intra-cavity signal power as the pump power is increased. If the pump polarisation is selected to be such that the idler and signal powers (P_i and P_s) remain constant at all pump levels, the heating remains constant too

2.2 Crystal absorption

As we have limited the intra-cavity signal power by using an output coupler mirror, there is a possibility that thermal effects in the OPO are not purely due to the signal absorption. Even in the linear cavity, in which the circulating field passes through the crystal twice per a round-trip, the maximum signal power in the crystal is below 300 W. The pump power can be close to 20 W and the idler power more than 3 W. Indeed, the signal power level is still more than an order of magnitude larger than the power levels of the other waves, but the crystal absorption may vary as a function of wavelength.

We studied the effect of pump absorption by varying the pump beam polarisation using a half-wave plate. This allowed us to increase the level of pump power without increasing the signal and idler powers. In practise, this was done by adjusting the half-wave plate so that the power of extraordinarily polarised pump light remained constant, independently of the total pump power. (The OPO is normally pumped with extraordinarily (e) polarised light. In the direction of ordinary (o) polarisation, the effective nonlinear coefficient is so small that the oscillation threshold cannot be reached. Crystal absorption is equal in both polarisations). The temperature increase ΔT in the crystal was deduced from the signal frequency change $\Delta\nu_s$, which was monitored using a wavemeter. By monitoring the signal wavelength, we can directly monitor the temperature variation seen by the beam, not only the crystal average temperature. The relationship between $\Delta\nu_s$ and ΔT was first measured by scanning the crystal temperature with the Peltier elements while simultaneously observing the signal wavelength shift. The relationship can also be calculated at reasonable accuracy from the phase matching condition using the available refractive index data [27].

An example of the temperature change versus pump power is shown in Fig. 4. When the generated idler and signal powers where limited to 0.3 W, increase of the pump power up to 18 W did not cause any notable temperature change. When operating the OPO normally with a purely e-polarised pump, a maximum temperature increase of 1–3 K was typically observed. This indicates that pump

absorption does not have any significant effect on the thermal load in the crystal. The same method can be used to check the effect of idler absorption. By changing the reflectivity of the output coupler mirror we can obtain conditions where the idler power for different cavity configurations is equal, but the intra-cavity signal power is different. We made such a comparison with two similar cavities, one with the $R \sim 98\%$ output coupler and the other one with a highly reflective mirror. The observed differences in crystal heating can be explained by the signal absorption solely, so the contribution of idler absorption on thermal effects is small.

The crystal absorption coefficient at signal wavelength can be estimated from the crystal heating measurements. Assuming radial heat flow and a constant heat-sink temperature, the radial temperature distribution $\Delta T(r)$ within the beam volume can be written as [28–30]

$$\Delta T(r) = k P_{\mathrm{s,c}} - \frac{\alpha P_{\mathrm{s,c}}}{2\pi K_{\mathrm{c}}} \frac{r^2}{w_{1\mathrm{s}}^2}, \tag{3a}$$

where

$$k = \frac{\alpha}{4\pi K_{\mathrm{c}}} \left(0.577 + \ln\left(\frac{2r_0^2}{w_{1\mathrm{s}}^2}\right)\right). \tag{3b}$$

The power absorption coefficient is denoted by α, $P_{\mathrm{s,c}}$ is the intra-cavity signal power, and r_0 is the radius of crystal aperture (i.e. half of the crystal thickness). Axial variation of the signal beam waist $w_{1\mathrm{s}}$ has been neglected for simplicity. Thermal conductivity of the congruent MgO-doped (5.0 mol%) lithium niobate is $K_{\mathrm{C}} = 4.02$ W/m K [31]. In the case of a linear cavity, we have to recall that the signal field passes the crystal twice per round-trip. This can be taken into account by multiplying $P_{\mathrm{s,c}}$ by two in (3a). When estimating the effect of power absorption on the phase matching condition, we can consider the on-axis temperature increase $\Delta T = \Delta T(0) = k P_{\mathrm{s,c}}$ only and neglect the radial gradient. This approximation is reasonable because the calculated radial temperature variation within the beam waist ($1/e^2$-intensity radius) is only ~20% for the configurations discussed here. We also tested various focusing conditions and observed no clear correlation between the focusing parameter(s) and crystal heating. This rather unexpected observation results from the fact that it is in practise impossible to build the cavity so that the beams would always hit exactly the same spot on the crystal when exploring different cavity configurations. As a consequence, there was substantial scattering in the measurement data, which was attributed to spatial variations of the crystal absorption. On average, the observed temperature increase versus signal power increase was $\Delta T/\Delta P_{\mathrm{s,c}} = 8$ mK/W and the respective standard deviation calculated from 12 independent measurements was 3.6 mK/W.

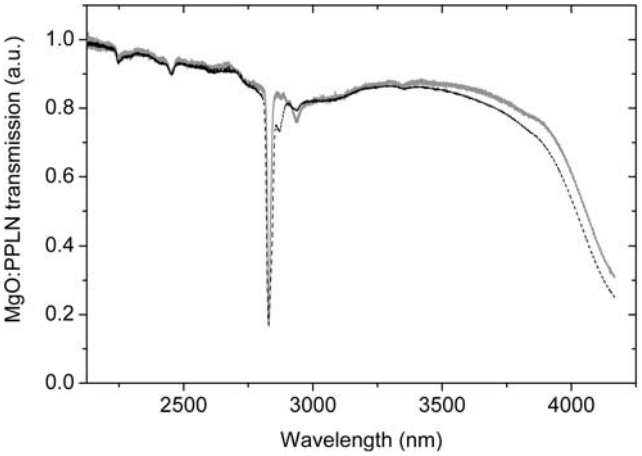

Fig. 5 Measured transmittance of the 5-cm long MgO:PPLN crystal used in the experiments. Measurements were done using an FTIR spectrometer. The solid grey curve was measured with extraordinarily polarised light and the black-dashed curve was measured with unpolarised light. The peak at 2.829 μm is due to OH-absorption. Origin of the smaller dips is unclear, but they were confirmed to be real by repeating the same measurements without the crystal

Using (3) and the measured value $\Delta T/\Delta P_{\mathrm{s,c}} = 8$ mK/W for the power dependence of crystal heating, we can estimate the crystal absorption coefficient α at signal wavelength $\lambda_{\mathrm{s}} = 1611$ nm to be

$$\alpha = \frac{4\pi K_{\mathrm{c}}(\Delta T/P_{\mathrm{s,c}})}{(0.577 + \ln(\frac{2r_0^2}{w_{1\mathrm{s}}^2}))} \approx 0.08\%/\mathrm{cm}.$$

The beam and crystal aperture radii $w_{1\mathrm{s}} = 75$ μm (average for the measurement set) and $r_0 = 0.5$ mm, respectively, were used in the calculation. The calculated absorption coefficient is the same as what has been previously measured at ~1800 nm using another method [14]. Due to the spatial variations of the crystal absorption, also the absorption coefficient given here should be considered as a spatially averaged value.

We did not perform any absolute measurements of the crystal absorption coefficient at the idler wavelength, but we did measure the relative variation of the crystal transmittance between 2125 and 4200 nm (Fig. 5). The measurement was done with a Fourier transform infrared (FTIR) spectrometer, first with unpolarised light and then separately with ordinary and extraordinary light polarisations. (Extraordinary polarisation is used in the OPO). Light was polarised using a Brewster polariser (Altechna, Lithuania) consisting of two Si-plates. The design wavelength of the polariser is 3 μm, but the extinction ratio was calculated to be >140 over the entire measurement region. Measurements of MgO:PPLN transmittance have been reported before, but only using unpolarised light and only for uncoated crystal samples [32]. We were interested to know also the effect of crystal anti-reflection coatings, so the measurement was

done with the same crystal that was used in the experiments published in this paper. Due to the large light beam (diameter ∼1 mm on the crystal facets) used in the measurement, the transmittance shown in Fig. 5 is a spatially averaged value, i.e. it does not reflect the spatial variations of the crystal absorption or coating quality.

The transmittance measurement of Fig. 5 reveals two distinct regions of large absorption: the phonon absorption at above 4 μm and the hydroxyl peak at 2.829 μm. (In lithium niobate the OH-peak is located at 2.87 μm, but it is blue shifted due to the MgO-doping of the crystal [33]). In this paper, we discuss only the wavelengths between these two highly absorbing regions, i.e. the band where we have confirmed that the thermal effects are strongly dominated by the signal absorption. It is, however, interesting to note that the OH-absorption peak is deep also for the e-polarisation. This result is different from the previously reported data for undoped PPLN [15], which at the wavelength of hydroxyl peak shows strong (>80%/cm) absorption of the o-polarisation but much smaller absorption (5%/cm) of the e-polarised light.

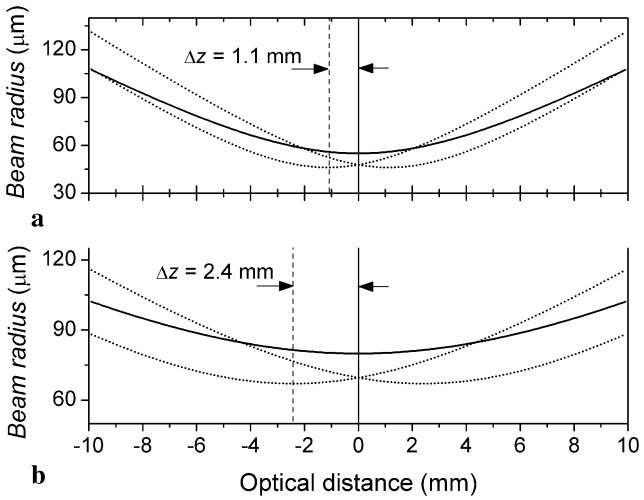

Fig. 6 Calculated effect of thermal lensing for two different waist sizes, (**a**) $w_{1s} = 55$ μm and (**b**) $w_{1s} = 80$ μm. For simplicity, the effect of astigmatism is neglected. Signal output power is 2.1 W and the crystal absorption coefficient is 0.08%/cm. Thermal lens produces two waists that are axially shifted with respect to the crystal centre (cold-cavity waist position). The shifts are denoted with Δz

3 Thermal effects

In this section we present an experimental study of some of the most important effects arising from the crystal heating caused by high intra-cavity signal power. First, we discuss thermal lensing that can lead to optical bi-stability. After that we consider the effect of crystal heating on the OPO spectral properties and investigate the conditions that need to be fulfilled in order to maintain stable OPO operation in a single longitudinal mode. Finally, we analyse the thermal self-locking effect that we have recently observed to exist also in SROs [11].

3.1 Thermal lensing and optical bi-stability

Although thermally induced refractive index gradient appears over the entire length of the crystal, it can be modelled by a thin lens placed in the middle of the crystal. A simple analytical model of thermal lensing can be obtained by considering a stationary Gaussian beam with boundary conditions similar to those used to derive (3). The advantage of this approach is that it is straightforward to include the thin lens into the ABCD-matrix of the cavity. Here we use the thin-lens model to qualitatively explain the experimental results of this section. We note, however, that a detailed theoretical study should take into account the gradual evolution of the thermal gradient due to thermally induced changes in the beam profile [34]. Also, the axial temperature gradient should be considered, as well as the effect of thermal lens on the pump beam. Altogether, such calculation would require an elaborate numerical model.

If the axial evolution of the beam is ignored, the effective focal length f_T of a thin thermal lens can be expressed as [28, 35]

$$f_T = \frac{\pi K_c}{\alpha P_{s,c}(dn_s/dT)} \frac{w_{1s}^2}{L_c}, \tag{4}$$

where $dn_s/dT = 5 \times 10^{-6}$ 1/K is the temperature dependence of the crystal refractive index [27, 36], and L_c is the crystal length. Again, we have to multiply the signal power by two when studying a standing-wave cavity. Due to symmetry of the cavity, there are two waists that are symmetrically shifted with respect to the crystal centre [26]. The calculated effect of thermal lensing for the cavity of Fig. 3 is shown in Fig. 6. For comparison, we have plotted the beam propagation also for another cavity that has a more loosely focused waist. As pointed out previously in Ref. [28], the cavity is more sensitive to thermal lensing the looser the focusing. However, as can be readily seen from (4), this sensitivity is partly compensated because the thermal lens becomes weaker (i.e. f_T becomes larger) as the waist size is increased.

An effect caused by thermal lensing can be seen in Fig. 7, which shows the OPO output power versus pump power. The curves in Fig. 7 were measured with otherwise exactly the same conditions, but with different axial positions of the pump beam focus in the crystal. In measurement A, the pump focusing lens was placed slightly (<5 mm) too far from the crystal, leading to an imperfect overlap of the pump beam waist and the OPO cavity (signal) waist. In measurement B, the pump focusing lens position was carefully optimised for the lowest possible threshold that corresponds to

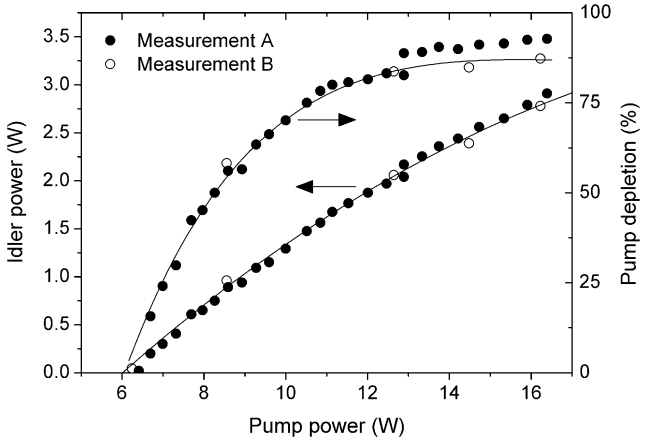

Fig. 7 Output power and pump depletion of the OPO of Fig. 3 measured as a function of the pump power. The focusing parameters of the pump and signal beams were $\xi_p = \xi_s = 2$. Measurement A shows a jump at $P_p \sim 13$ W caused by thermal lensing. In measurement B no jump exists because the axial overlap of the pump and signal beams is better optimised. The solid lines are guides for the eye

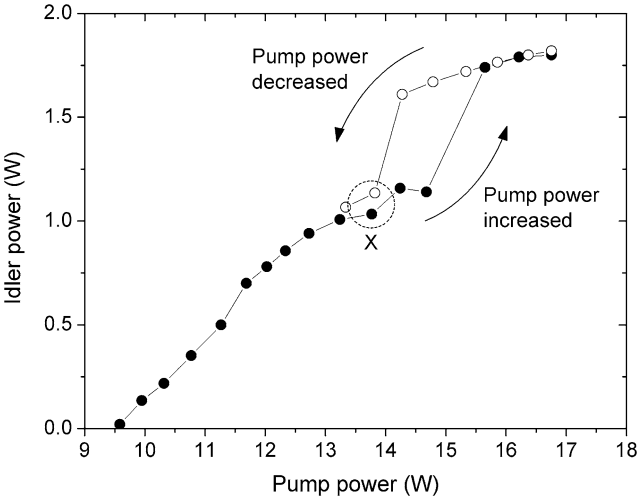

Fig. 8 Bi-stability observed with a linear four-mirror OPO cavity that was constructed to provide a focusing parameter $\xi_s = 0.6$ ($w_{1s} = 100$ μm at 1611 nm wavelength). The pump beam was more tightly focused with $\xi_p = 2$. The point of bifurcation (X) moves to a lower pump power as the cavity mode waist size is increased by decreasing the cavity arm length d_2

the best spatial overlap of the two interacting beams. When the OPO power is increased, thermal lensing shifts the beam focus in the cavity (Fig. 6), leading to a small but distinct jump in the OPO output power and pump depletion of measurement A. The jump was reproducible and it corresponds to a situation where the pump and signal beams find a better overlap due to the thermal lens. (It is interesting to notice that such a jump can be seen also in an early report on SROs [6]). As the focusing condition of measurement B was optimised for the optimum overlap for the cold cavity, a smooth increase of the OPO output is observed instead of the jump. We studied the OPO behaviour by changing the cavity dimensions (signal waist size) and found that, regarding the jump, the OPO is insensitive to such variations. Instead, changes as small as a few millimetres in the axial position of the pump focus relative to the signal focus cause change in this behaviour. The observed effect is hence explained by axial mismatch in the pump-signal beam overlap, not by a mismatch of the focusing parameters ξ_s and ξ_p.

With some configurations, the jump in the OPO power was accompanied by a bi-stable region (Fig. 8). In particular, bi-stability can occur if the signal waist size is large. This is understandable, since the axial shift of the waist position due to thermal lensing increases with the waist size. We changed the cavity arm lengths d_2, which changes the signal waist size. Increase in the waist size pushed the bifurcation point X of bi-stable region (Fig. 8) to a lower pump power and made the bi-stable region larger. On the other hand, wide bi-stable region could be most easily observed if the pump beam focusing parameter was significantly different from that determined by the signal cavity. For instance, in the case of a loose signal cavity focus of Fig. 8, tight pump beam focusing resulted into a wide bi-stable region. Although the exact reason for this is unclear, it seems that the width of the bi-stable region depends on the mismatch between the (cold-cavity) parameters ξ_s and ξ_p, while the existence of such effect correlates with the axial mismatch of the beams.

The same kind of bi-stability as shown in Fig. 8 has been previously reported to exist with triply resonant OPOs [37], and recently also with a SRO in which the idler wave is resonated instead of the signal wave [16]. The latter publication [16] reports an interesting experimental observation of a sudden inset of thermal guiding, which is associated with the jump to the high-power state of bi-stability. To the best of our knowledge, bi-stability has not been previously reported for a SRO that resonates the signal wave, except for a hybridly pumped SRO that contains additional gain material within the cavity [38]. This is probably because the effect is small and difficult to observe if a cavity with small waist size ($\xi_s = 1$ or larger) is used, which usually is the case. For instance, in the measurement of Fig. 7, we did not observe any bi-stability at the point of power jump. It is possible that bi-stability exists but the region is so narrow that it is below our measurement resolution (about 0.15 W in pump power). We have observed bi-stability only with the four-mirror linear cavity, not with the ring cavity. This is attributed to the larger temperature increase in the linear cavity. The larger temperature increase occurs because in a linear cavity the signal beam passes the crystal twice per round-trip, making the absorbed power approximately 1.5 times as large as that in the ring cavity, even if the circulating power is somewhat smaller due to the extra mirror losses. In the idler-resonant SRO, strong bi-stability was observed with a ring

cavity [16], which is presumably due to large absorption at the idler wavelength. Furthermore, in idler-resonant OPOs the large difference between the pump and resonance wavelengths can more easily lead to a spatial mismatch between the two beams [16].

To summarise, we have experimentally confirmed that it is possible to minimise the effect of thermal lensing by using a small waist size of the cavity mode. Elimination of the thermal lensing allows for high parametric conversion efficiency at all power levels. We have found that the lowest threshold and the highest pump depletion (90 to 95%) is obtained with tightly focused beams, $\xi_p = \xi_s = 2$. Another suggested method for making the cavity less sensitive to thermal lensing is to adjust the cavity dimensions closer to a cold-cavity stability limit [39]. (In Fig. 3, this would correspond to a d_1 longer than that of the stability centre). A problem related to this method is that it can lead to an unstable cavity at low power levels [26, 39]. Also, accurate modelling of the thermal lensing effect becomes laborious. If the temperature increase is modest, a simple model of a static thermal profile following from the Gaussian beam profile can give reasonable results [39].

3.2 Spectral instabilities

With the signal output coupler ($R \sim 98\%$) and a good quality MgO:PPLN crystal, the OPO remains stable single mode up to the highest available pump power of ~18 W [11]. The spectral purity of the OPO is very good; side modes are typically suppressed by 23–27 dB. Stable operation can be obtained over the entire tuning range, which for the idler wavelength was measured to be 2.7–3.45 μm. Although our current setup does not allow tests at wavelengths closer to the degeneracy, it is expected that instabilities start to arise when approaching it. This is because the parametric gain profile becomes wider and cannot provide sufficient frequency selectivity any more. In practise, reliable mode-hop-free operation requires some shield against airflows that can disturb the cavity frequency by more than $FSR/2$ (100 MHz). We have used a plexiglass cover during the measurements reported here. By decreasing length of the linear cavity to about 370 mm, which corresponds to $FSR \sim 400$ MHz, it is possible to have reliable long-term single mode operation also without the cover. The drawback is that, with the given concave mirrors, this inevitably leads to a larger cavity mode waist size (~100 μm) and thus to a less efficient parametric conversion process.

The risk of spectral instabilities increases with the increase of OPO power. We have observed two distinct regions of spectral instabilities. These regions are depicted in Fig. 9, which shows the optical spectrum of the OPO measured at different pump levels. To reach high enough intracavity power levels to induce instabilities, we have used a highly reflective ($R > 99.9\%$) mirror instead of the partially transmitting output coupler. The first transition away from pure single mode operation is observed at about 6 W pump power, after which side modes start to arise. The number of side modes is small, most commonly there are only two or four of them. The side modes are also weak compared to the main mode, but they get larger with the increase of pump level. In most cases, the side modes are not the adjacent longitudinal modes of the signal cavity. Instead, they are separated from the main mode by several GHz. It has been proposed that multiple OPO modes are related to higher order transversal cavity modes, arising from thermal effects in the crystal [34]. We have not been able to confirm if the side modes are of higher transversal order but, indeed, we have observed them to be related to temperature increase in the crystal. Typically the side modes start to arise after 1 to 1.5-K temperature increase. As was already mentioned, shielding the cavity with a plexiglass cover can reduce this tendency. When using the optimised linear cavity (Fig. 3) with 4%/round-trip output coupling, crystal heating can be kept below the critical level by selecting a spot of low absorption in the crystal. On average, however, the temperature

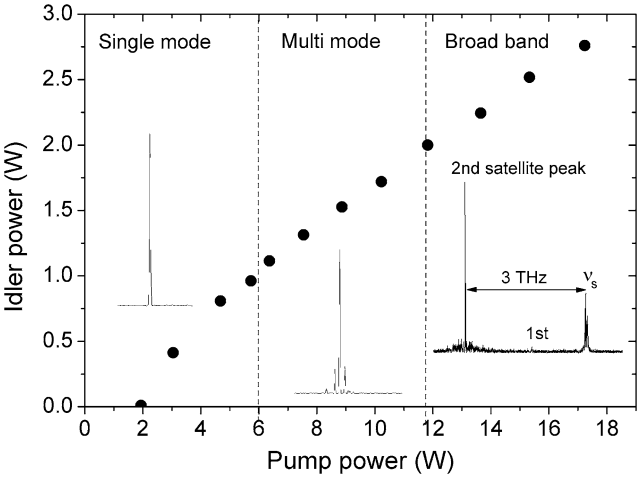

Fig. 9 Three regions of different spectral behaviour are observed when increasing the pump power of an OPO that has a high-finesse signal cavity consisting of four highly reflecting ($R_s > 99.9\%$) mirrors. All the spectra shown in the insets are plotted with linear power scales. In the low power region, the OPO operates in a single longitudinal mode with the side modes suppressed by more than 20 dB. At intermediate power levels the OPO operates in a few multiple longitudinal modes, and the side modes get stronger with the increase of power level. In the high power region the number of side modes significantly increases and also strong satellite peaks exist [40]. The OPO signal frequency is denoted by ν_s. Often a weak 1st satellite peak started to appear already at approximately $P_p = 10$ W, but it was observed more consistently at $P_p = 11 \ldots 12$ W. For $P_p = 12$ W the 1st satellite peak is dominant, but the 2nd peak gets stronger as the pump level is increased. The spectrum was recorded at $P_p = 15$ W (a large number of side modes exists around the main peaks, but their separation is in the order of a GHz and hence they are not well resolved at the scale of the *inset*)

increase corresponding to the maximum OPO power is approximately 2 K. This suggests that even larger output coupling should be used in order to ensure reliable single mode operation in all cases without the need for selecting a good spot on the crystal.

If the OPO pump level is further increased, there is a transition to broadband multi-mode operation. The spectrum of the multi-mode state depends on the configuration and on the OPO power level. Sometimes the spectrum is a comb of several distinct and strong cavity modes that are a few GHz apart from each other, and sometimes it is a wide continuum of closely spaced modes. In addition to the several strong side modes, one or two satellite peaks far away from the original OPO frequency often exist (Fig. 9). This behaviour is similar to that reported before in references [40, 41], in which it was attributed to Raman lasing. The transition to broadband oscillation typically occurs at pump levels 3.3–5 times the OPO threshold, depending on the cavity configuration.

3.3 Thermal locking

The oscillation frequency of the SRO is, ideally, determined by a combination of only two gain components: the parametric gain curve and the comb of longitudinal cavity modes. This situation is schematically depicted in Fig. 10. In a conventional SRO, the total gain is further modified by an intra-cavity etalon, which usually has a spectral linewidth of the same order of magnitude as that of the parametric gain curve. The parametric gain curve is wide (>100 GHz) compared to the spacing of the cavity modes (<1 GHz). The OPO oscillates at the cavity mode that experiences the largest net gain, i.e. close to the maximum of the parametric gain curve. In order to avoid mode hops, the frequency fluctuations between the cavity modes and the parametric gain curve should not exceed $FSR/2$, on average. Such fluctuations can be caused by ambient perturbations, such as air flows or thermal expansion that vary the optical length of the cavity. The most stringent requirement is set by the temperature stability of the nonlinear crystal. Temperature variations of the crystal change via thermal expansion and temperature dependence of the refractive index the cavity frequency and the position of the parametric gain curve. Of these two, the latter shift is more significant. Approximately in the middle of our OPO tuning range ($\lambda_s = 1611$ nm) the measured shift of the gain curve versus temperature is -60 GHz/K, and the shift in cavity frequency is approximately -0.5 GHz/K. This means that, in order to avoid mode hops, the crystal temperature stability should be of the order of 1 mK.

In our OPO, the (average) temperature of the crystal is stabilised to within 12 mK, and yet the OPO can be operated without mode hops for several hours. In fact, the OPO can tolerate temperature fluctuations of the order of 100 mK

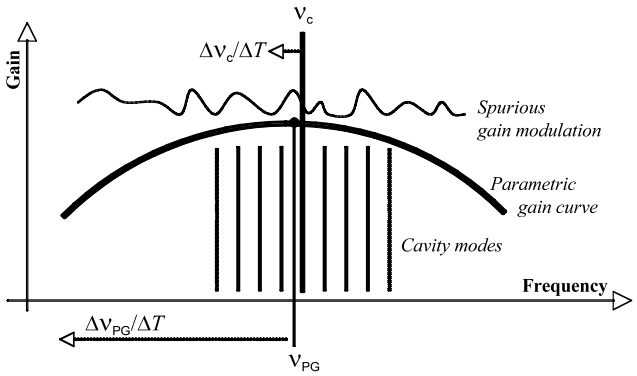

Fig. 10 Principle of signal frequency selection in a singly resonant OPO. In the ideal case, the oscillation frequency is determined by the parametric gain curve and the cavity resonance modes. The cavity mode (ν_c) closest to the gain curve maximum (ν_{PG}) is the one that oscillates. In practise, the gain curve is modified by spurious frequency selective losses, see text for details. Crystal temperature variations shift the frequencies of the cavity modes and the parametric gain curve, which is indicated by *arrows* in the figure

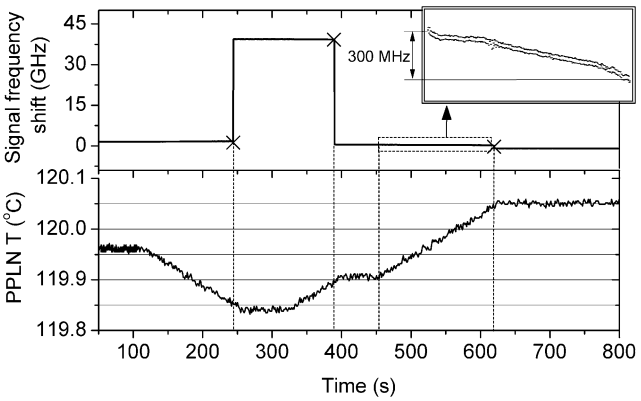

Fig. 11 Signal frequency deviation versus crystal temperature tuning. Depending on the actual gain profile around the operation point of the OPO the crystal temperature can be changed by several tens of mK before a mode hop occurs. The mode hops are denoted by crosses in the upper panel. The inset shows the signal frequency drift during a linear temperature scan. The nonlinear frequency change can be explained by a thermal self-locking effect, see text for details

without a mode hop, which is demonstrated in Fig. 11. There are at least two effects that can account for the observed insensitivity of the OPO to thermal fluctuations. First, the parametric gain profile of the OPO is flat and the resonance condition is hence affected by any frequency dependent loss that modifies the gain profile. Second, we suggest that a thermal self-locking effect related to absorption in the nonlinear crystal can be strong enough to compensate for small frequency fluctuations.

We have carefully suppressed all residual etalons within and outside of the OPO cavity, because such etalons can deteriorate the OPO wavelength tuning properties. We have also used cavity mirrors that are anti-reflection coated for the idler wavelength in order to avoid modal competition with

the signal cavity modes. The signal–idler clustering should not be a problem anyway, as the signal–idler mode spacing, calculated from $FSR_i \times FSR_s/(FSR_i - FSR_s)$, is approximately 60 GHz. This is of the same order of magnitude as the half-width of the parametric gain curve. Despite these considerations, the actual parametric gain curve is not perfectly smooth (Fig. 10). Residual modulation of the gain can be seen as a small (max. few %) power variation when tuning the OPO cavity length or when including an intra-cavity etalon and tuning the wavelength by tilting it. Also, when tuning the wavelength by changing the crystal temperature, the mode hops often are much larger than the cavity mode spacing. Spacing of the mode-hops varies, but they often occur in multiples of 6 GHz. This does not correspond to any obvious parasitic etalon in our setup, but could be due to a multiple of the mode spacing of an etalon formed between the crystal surfaces ($FSR \sim 1.5$ GHz), for instance. In addition to the possible etalon effects caused by imperfect AR-coatings, gain modulation can be caused by irregularities in the nonlinear crystal. It has also been suggested that, in a standing-wave cavity, additional mode selection could arise due to different losses on crystal surfaces depending on if the signal wave nodes or antinodes are located on the crystal surfaces (where optical losses are typically larger than within the crystal) [42].

Although the modulation of parametric gain is small, it provides additional frequency selectivity that reduces the tendency for cavity mode hopping and multimode operation. Another effect that might improve the OPO frequency stability is the thermal self-locking effect, which has been previously observed in doubly and triply resonant CW OPOs [43–45]. It has helped to achieve mode-hop free operation of up to 24 h with a freely oscillating doubly resonant OPO [45]. Thermal locking is known to exist in other kind of laser systems, too. A detailed analysis of the locking phenomenon for a system consisting of an optical Fabry–Perot cavity filled with an absorbing gas sample is presented in Ref. [46].

In the SROs, thermal locking owes to the small temperature change in the nonlinear crystal due to absorption of optical power. If the cavity frequency ν_c drifts relative to the parametric gain curve, there will be a small change in the circulating intra-cavity field and hence also in the absorbed power. The corresponding change in the crystal temperature (within the beam volume) shifts the parametric gain curve. The direction of the gain curve shift is towards a higher frequency when the temperature decreases, and hence the locking can occur if the cavity frequency ν_c is blue-detuned from the gain maximum ν_{PG} (Fig. 10). The parametric gain curve will follow the cavity frequency drift, i.e. the thermal effect will partly compensate for the drift $\Delta(\nu_c - \nu_{PG})$. If the OPO originally oscillates on the red-detuned side of the parametric gain curve, it has a tendency to make a mode hop to the blue-detuned side as the thermal effect shifts the parametric gain curve to the opposite direction compared to the cavity frequency drift.

In the following, we present a simple calculation of the thermal locking range using the notations shown in Fig. 10. We first assume that the parametric gain curve is smooth and that the OPO initially oscillates at the frequency of maximum parametric gain, so that $\nu_c = \nu_{PG} = \nu_{ini}$, where ν_{ini} is the initial (reference) frequency. In addition, the temperature dependence ($\Delta\nu_c/\Delta T = -0.5$ GHz/K) of the cavity frequency is much smaller than that of the parametric gain ($\Delta\nu_{PG}/\Delta T = -60$ GHz/K). We can hence ignore the fact that also the cavity modes are slightly shifted due to crystal temperature variations (or, we can subtract of the temperature dependency of the cavity frequency from that of the parametric gain curve). For simplicity, we use a Gaussian profile as an approximation for the gain curve. This is a good approximation when operating the OPO close to the parametric gain maximum, which is the case when no frequency selective intra-cavity element (etalon) is used. The intra-cavity signal power $P_{s,c}$ can thus be written as

$$P_{s,c} = P_{s,cM} \exp\left(-2\sqrt{2}\frac{(\nu_c - \nu_{PG})^2}{\Gamma_{PG}^2}\right), \tag{5}$$

where $P_{s,cM}$ is the maximum intra-cavity signal power obtained when the oscillating cavity mode overlaps with the centre of the parametric gain curve. Width Γ_{PG} (FWHM) of the parametric gain curve can be calculated from the group velocity indexes of the pump, signal and idler waves [27].

If the crystal heat sink temperature is T_c, the temperature seen by the signal beam is $T_c + \Delta T$, where $\Delta T = \Delta T(0)$ is the on-axis temperature increase caused by signal absorption. Using (3a), the deviation δT from the temperature $T_c + \Delta T_{ini}$ that corresponds to the initial state $\nu_c = \nu_{PG} = \nu_{ini}$ can be expressed as

$$\delta T = (T_c + \Delta T) - (T_c + \Delta T_{ini}) = k(P_{s,c} - P_{s,cM}). \tag{6}$$

As the crystal temperature varies, the frequency of maximum parametric gain shifts from the initial value ν_{ini} according to

$$\nu_{PG} = \nu_{ini} + C_1 \delta T, \tag{7}$$

where $C_1 = \Delta\nu_{PG}/\Delta T$ is the temperature coefficient of the (signal) phase matching frequency in GHz/K. This coefficient depends on the wavelength and, as was already mentioned, we have measured it to be -60 GHz/K at $\lambda_s = 1611$ nm.

Using the three coupled equations, (5)–(7), we can express the steady state frequency difference between the os-

cillating cavity mode and the maximum of the gain curve as

$$\nu_c - \nu_{PG} = \sqrt{\frac{\Gamma_{PG}^2}{-2\sqrt{2}} \ln\left(1 + \frac{(\nu_{PG} - \nu_{ini})^2}{kC_1 P_{s,cM}}\right)}. \quad (8)$$

Noting that the cold cavity detuning $\delta\nu_c = \nu_c - \nu_{ini}$ can be written as $\delta\nu_c = (\nu_c - \nu_{PG}) - (\nu_{PG} - \nu_{ini})$, (8) can be used to estimate how the frequency of maximum parametric gain varies versus cavity detuning, i.e. how well the thermal locking effect is capable of compensating for drifts between the cavity mode and the parametric gain. It turns out that, in the ideal case of a smooth parametric gain curve, the thermal effect can compensate only a few percent of the drift. This is due to the wide ($\Gamma_{PG} = 150$ GHz) and flat parametric gain profile. Without an intra-cavity etalon, the OPO always oscillates close to the parametric gain curve maximum, where the derivative $dP_{s,c}/d(\nu_c - \nu_{PG})$ is small and thus also the thermal correction subsequent to a cavity detuning is small.

In practise, the thermal locking effect is amplified by the spurious variations of the parametric gain curve that make $dP_{s,c}/d(\nu_c - \nu_{PG})$ larger (Fig. 10). If we study frequency variations that are small compared to the period of local variations of the gain curve, we can approximate a local maximum by a Gaussian function. If we assume that the parametric gain profile shifts without changing its shape, we can estimate the effect of thermal locking directly by using (8). Now we just replace the width of the ideal parametric gain curve with that used to approximate real, modulated, gain profile. An example of such calculation with a gain curve with $\Gamma_{PG} = 3$ GHz is shown in Fig. 12. The other parameter values used in the calculation are those deduced from experiments, and they are given in the figure caption. The calculation shows that the cold-cavity detuning can be larger than $2 \times FSR$ before the frequency difference between the cavity frequency and the parametric gain maximum exceeds $FSR/2$ and a mode hop occurs. This is in agreement with our experimental observations that the maximum mode-hop-free tuning obtained by scanning the cavity length with a PZT can be more than $2 \times FSR$. A cold-cavity detuning of $2.25 \times FSR$ (Fig. 12) can be compensated by a temperature change δT of about 6 mK, which with the operation conditions of Fig. 12 corresponds to a power change of as small as 0.35%. This too is in agreement with the typically observed power variation (<1%) during the frequency scans.

If the gain curve is modified by parasitic etalon effects, the assumption that the local gain maxima shift by the same amount as the ideal gain curve is not valid any more. If we consider small frequency drifts, we can ignore the slowly varying background caused by the ideal parametric gain profile and assume the thermal correction arising from the thermal shift of the cavity mode (−0.5 GHz/K) relative to the residual etalon mode. Note that in this case the locking occurs on the red-detuned side of the local gain maximum,

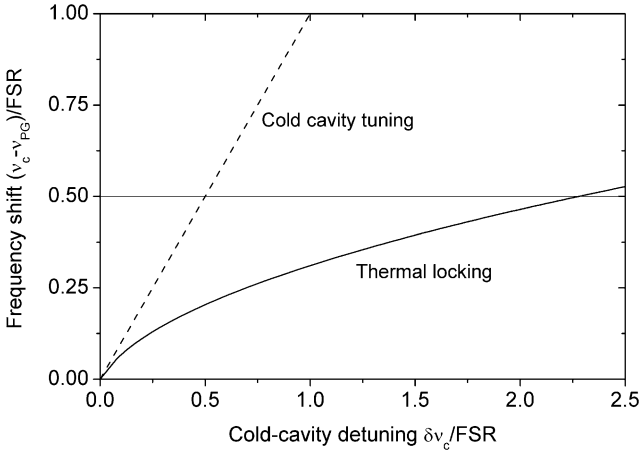

Fig. 12 Thermal locking range calculated using (8). The frequency scales are normalised with the cavity free spectral range $FSR = 210$ MHz. In the absence of thermal locking, the cold-cavity frequency can be detuned from the parametric gain maximum by $0.5 \times FSR$ until a mode hop occurs. Thermal locking resists the cold-cavity tuning (cavity length scanning) and the cold-cavity frequency can be detuned by $2.25 \times FSR$ without a mode hop. (Mode hop occurs when the OPO cavity mode ν_c is shifted by $0.5 \times FSR$ relative to the parametric gain maximum ν_{PG}). The cavity is a linear four-mirror cavity (Fig. 3) with an output coupler that transmits 2% of the signal power. Signal output power is 2 W, signal absorption coefficient is $\alpha = 0.08\%/\text{cm}$, waist size is $w_{1s} = 55$ µm, and the crystal aperture is $r_0 = 0.5$ mm. The calculation assumes a locking to a local gain maximum that can be modelled with a Gaussian profile that has a width of $\Gamma_{PG} = 3$ GHz (FWHM). Parametric gain curve shift versus temperature is $C_1 = -60$ GHz/K and thermal conductivity of the crystal is $K_C = 4.02$ W/m K

which is opposite to that discussed above for the case in which the parametric gain curve shift is responsible of locking. If it is thermal shift of the cavity frequency that provides the negative feedback, a local gain maximum with a FWHM of approximately $2.5 \times FSR$ is needed to compensate for a cold-cavity drift of $\delta\nu_c \sim FSR$. Due to the relatively small temperature dependence of the cavity mode, the locking over such a large range requires a temperature change of −200 mK, which corresponds to a signal power drop by more than 10%.

In most cases the experimentally observed power drop is below 1% when scanning the cavity length, which suggests that the thermal locking effect is dominated by the parametric gain curve shift. However, sometimes large and sharp power variations are observed. This is demonstrated in Fig. 13, which shows the idler output power measured while scanning the OPO cavity length with a triangular waveform. The measurement was done using a two-mirror cavity that is shorter (0.3 m) than the four-mirror cavity (0.7 m). Because the ratio of the crystal length to the total cavity length is larger, also the temperature dependence of the cavity mode becomes larger (−1.25 GHz/K). This makes the thermal locking effect stronger. The observed mode-hop-free tuning range of $0.65 \times FSR$ can be explained by a 70-mK temper-

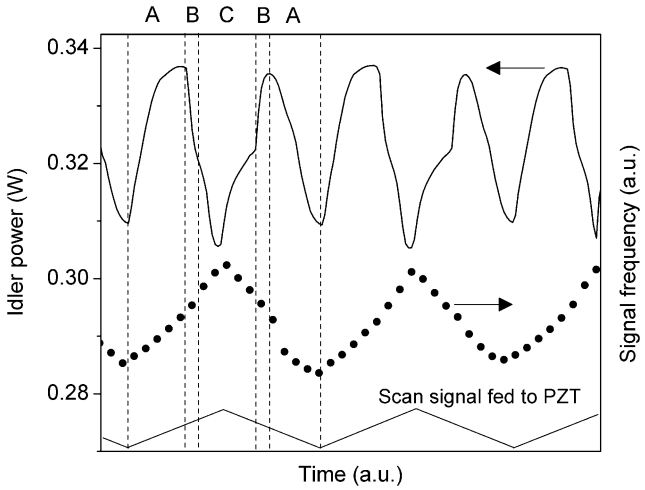

Fig. 13 Idler power and signal frequency variation as the OPO cavity length is scanned with a triangular wave applied to a PZT element that is attached to one of the cavity mirrors. Under strong thermal locking to a narrow local maximum of the gain curve, asymmetric power pattern is observed. The width of the pattern depends on the direction of cavity length scan. Also the frequency tuning becomes nonlinear. See text for the explanation of regions A–C

ature compensation that corresponds to a 4% power drop, as calculated using (5)–(6). This is in reasonable agreement with the observed ∼7% power drop, especially when considering that we have used the spatially averaged value of absorption coefficient in the calculation.

The pronounced asymmetry of the output power versus cavity detuning in Fig. 13 is similar to that observed in doubly resonant OPOs under thermal locking [28, 44, 45]. Thermal locking takes place within the region A, which can be seen as a slow variation of the output power. As the cavity frequency becomes blue-detuned relative to the local gain maximum, the thermal effect accelerates the scanning rate and the output power drops quickly (region B). The same phenomenon causes the nonlinear tuning of the signal frequency, which is evident in Fig. 13 despite the slow sampling rate (1 S/s) of the wavemeter. From the fact that locking occurs on the red-detuned slope, one can conclude that the effect is due to thermal shift of the cavity mode rather than that of the parametric gain curve. On the other hand, the region C in Fig. 13 shows a locking behaviour that has opposite sign compared to the region A. It is thus probable that within this region the dominating effect is the thermal shift of the parametric gain curve. Altogether, the shape of the gain profile is likely to be caused by a combination of more than one effect, in which case the calculation of thermal locking range should take into account temperature dependencies of the individual gain components (also the spurious etalon modes may shift vs. temperature). However, most of the experimental observations can be satisfactorily explained with the simple model presented above. It shows that small variations of the parametric gain profile can enhance the thermal locking effect so that frequency fluctuations larger than a cavity *FSR* can be compensated for.

Figure 13 is presented here because it strongly suggests that the observed self-locking phenomenon is of thermal origin. Normally the OPO power variations are much smaller and less sharp so that the asymmetry in output power versus detuning cannot be observed. The self-locking effect can be most easily observed as a tendency of the OPO to resist frequency tuning. This leads to nonlinear signal frequency tuning when the crystal temperature or the cavity length is scanned. This kind of behaviour can be seen in Fig. 13, as well as in the inset of Fig. 11, which shows the signal frequency as a function of a linear scan of the crystal temperature. The actual tuning rate depends on the OPO operation point and on the smoothness of the gain curve. At some operation points, the signal frequency remains essentially constant during the entire scan until a mode hop occurs. The self-locking effect was observed also with a four-mirror OPO that had a 400-μm thick uncoated YAG etalon placed within the cavity. Due to its more complex structure and behaviour, we did not explore the etalon-OPO in detail. However, some small differences compared to the etalon-free design can be expected. First, the additional frequency selectivity provided by the etalon can help to reduce the effects of spurious gain modulation that are evident in our etalon-free OPO. Secondly, the etalon allows one to tune the OPO wavelength significantly away from the parametric gain maximum, so that the slope of the parametric gain curve becomes steeper. This can be expected to enhance the thermal locking effect at some operation points.

To summarise, we have presented several measurements that indicate the OPO's tendency to resist frequency tuning. Such behaviour is known from previous reports of other groups, and different explanations for it have been proposed. For instance, the nonlinear tuning characteristics have been attributed to thermal and photorefractive effects in the nonlinear crystal [17]. Our observations and analysis support the hypothesis that such behaviour is caused by a thermal self-locking effect. A paper recently published by another group reports an observation of a similar, but much stronger, self-locking effect with an idler-resonant SRO [16]. Although many of the reported experimental results can be qualitatively explained by the thermal self-locking phenomenon, it is worth noting that the possibility of other contributing effects cannot be excluded, and that more work needs to be done to get comprehensive understanding of the tuning characteristics of the singly resonant OPOs.

4 OPO stability and tuning

In this section we report the stability and tuning characteristics of a SRO under thermal loading. We mainly discuss the

4-mirror linear-cavity OPO shown in Fig. 3, but the results also apply to the two-mirror cavity OPO that has been previously described in Ref. [11]. We have stabilised the crystal temperature to within 12 mK and reduced the intra-cavity signal power by using the partly transmitting output coupler. The good thermal control ensures stable single mode operation also at high output power levels and provides good wavelength tuning properties. However, the tuning and stability of the OPO are still affected by the thermal effects discussed in the previous section.

4.1 Stability

During the first 45–60 min after turning on the pump laser, the OPO often makes some mode hops which are related to warm-up of the pump laser (Fig. 2). After the warm-up period and with the OPO parked at a single frequency, mode-hop free operation over several hours can be consistently obtained. In our previous study we reported a mode-hop free operation of more than 20 h [11]. In general, long-term frequency drifts can stem from ambient temperature and pressure variations, as well as from relaxation of mechanical stress. In our current setup the major effect was observed to be thermal expansion of the cavity baseplate, which is not temperature stabilised. An example of a drift caused by thermal contraction is shown in Fig. 14, which shows an overnight recording of the OPO frequency an power. There is no clear correlation between the signal frequency and the idler power. This can be because the idler power is affected not only by the cavity drift but also by the pump power. The long-term (in)stability of the pump laser is in the order of 1%, which converts to approximately same relative drift in idler power. The lack of correlation between the signal frequency and the idler power could also be explained by the thermal locking effect, which attempts to minimise the frequency drift between the cavity resonance and parametric gain maximum, hence trying to maintain a constant OPO power. (Thermal lock is not an absolute frequency stabiliser). This explanation is supported by the fact that the observed mode-hop-free drift of the OPO frequency is almost twice as large as the cavity *FSR*. Thermal locking could also explain the temporal variation of the level of power fluctuation, because the strength of the thermal lock depends on the operation point and the gain of the lock varies with the frequency drift. (Power fluctuation slightly increases at the end of the measurement, see Fig. 14). However, it is also possible that transmission maxima of the parasitic etalons drift with temperature so that it follows the drift of the cavity resonance frequency. This could lead to behaviour similar to that observed in Fig. 14. The increase in noise would then be just mode-transition noise similar to that often observed in lasers. (Although we have confirmed that the side-modes are suppressed by a factor of 100, at least, during the entire measurement).

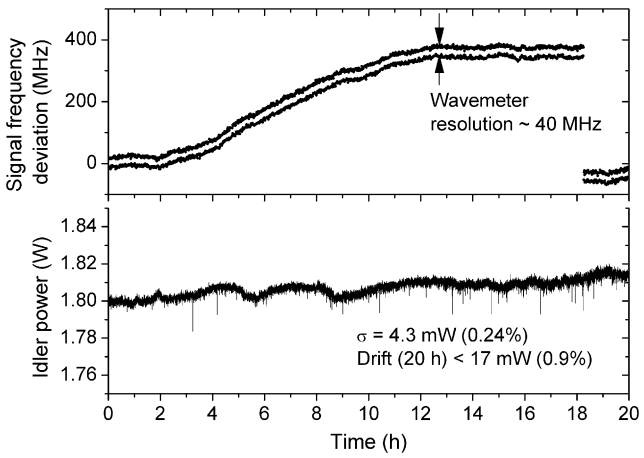

Fig. 14 Long-term frequency and power stability of the 4-mirror linear-cavity OPO (Fig. 3) measured overnight, demonstrating mode-hop-free operation of more than 18 h. The focusing parameters of the pump and signal beams are $\xi_p = \xi_s = 2$. Sampling interval is 1 s, and the crystal poling period is 31 μm. The pump power is 13.5 W, which is 2.1 times the threshold power. The drift in signal frequency is caused by thermal contraction of the cavity baseplate. The decrease in laboratory temperature during the measurement was ∼0.2 K

Typical long-term drifts observed in laboratory conditions are similar to those shown in Fig. 14. Over a time period of several hours, the frequency drift is usually less than a cavity *FSR* (210 MHz), and the idler power drift is smaller than 1%. In a short term, signal frequency fluctuations as large as 100 MHz were observed due to acoustic noise. Shielding of the OPO cavity with a simple plexiglass cover reduced these fluctuations below the resolution (∼40 MHz) of the wavemeter. If the ambient conditions remain constant, the OPO frequency can remain within 50 MHz for more than ten hours, which was demonstrated in our previous work [11].

4.2 Wavelength tuning characteristics

The idler wavelength can be scanned continuously within the wavelength region supported by a single poling period by combining a stepwise crystal temperature scan with a mode-hop-free wavelength scan of the pump laser. First, the crystal temperature is stepped so that the signal and idler frequencies make discrete jumps of opposite signs. After the step, the signal frequency is kept constant while the pump laser frequency is scanned. According to the principle of energy conservation, $\nu_i = \nu_p - \nu_s$, the idler frequency follows the pump frequency scan. If the step sizes in signal frequency are kept smaller than the tuning range (140 GHz) of the pump laser, the successive pump laser scans overlap with each other and the idler wavelength is scanned continuously without gaps.

The simple temperature tuning method is demonstrated in Fig. 15 by scanning over a frequency range of 6.5 THz

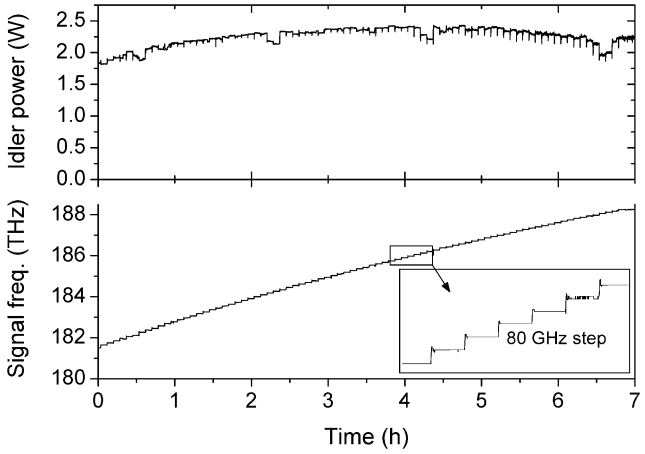

Fig. 15 Stepwise wavelength scan over 6.5 THz with the 4-mirror linear-cavity OPO (Fig. 3). The focusing parameters of the pump and signal beams are $\xi_p = \xi_s = 2$. The scan was done by stepping the MgO:PPLN temperature by −1.25 K after every five minutes. Usually single-mode operation is restored quickly after a temperature step, but at the regions of increased crystal absorption the stabilisation takes longer and mode hops can appear still few minutes after the step (*inset of the lower panel*)

(217 cm^{-1}). The frequency step size changes over the scan due to the MgO:PPLN dispersion. This is a well-known effect that can be taken into account in the automated scanning process. Due to the frequency dependent losses (residual etalon effects, crystal irregularities, etc.) there are also some local variations of the step size, which is shown in the inset of Fig. 15. Such variations are small compared to the tuning range of the pump laser, so they do not prevent reliable and continuous idler scanning. Tuning range was limited by the maximum operating temperature (120°C) of the Peltier elements used in crystal temperature control. It is expected that the tuning range could be further increased by using Peltier elements with >200°C temperature rating [45]. Tuning over at least 450 cm^{-1} should be possible, as it has been previously reported with an etalon equipped SRO [2], which is inherently susceptible to reduction of the tuning range due to the etalon walk-off losses. Mirror and crystal coatings do not limit the continuous tuning range, as their properties remain essentially constant over the signal and idler wavelength regions of 1.54–1.76 μm and 2.7–3.45 μm, respectively. The effect of coatings on the OPO output power versus wavelength tuning is small, as well. The power variation observed in Fig. 15 is mainly due to changes in cavity alignment when the crystal temperature is varied. This stems from the temperature dependence of the crystal refractive index. We have used a nonlinear crystal with 1°-wedged faces, and as the beam incidence angle differs from normal incidence, any change in the crystal refractive index varies the beam path in the cavity. This hypothesis is supported by the fact that the maximum output power can be restored at any point of the scan by realigning the cavity for that particular point. After the realignment, the maximum power is obtained at the temperature for which the alignment was done, while the other operation points suffer a power drop. The overall power drop during a long wavelength scan can be minimised by aligning the cavity with a crystal temperature that corresponds to the centre of the tuning range (Fig. 15). If the alignment is done at one end of the tuning range, the power drop can be as large as 50% [11]. In future setups, the thermally induced cavity misalignment could probably be reduced by using a nonlinear crystal which has facets with smaller wedge angles.

Another distinct feature in Fig. 15 is the existence of spectral regions where the OPO output power drops by a few percent. This behaviour is repeatable from scan to scan, as well as the region of increased power fluctuations at the high frequency end of the scan. This behaviour is attributed to bad spots in the crystal. By slightly translating the crystal it was possible to reduce the power drops, although they could not be completely removed. These power drops were not observed in the crystal transmittance measurements (Sect. 2.2) done with the FTIR spectrometer at the signal and idler wavelengths—however, those measurements only represent a spatially averaged value of the crystal transmission, as the light beams used in the measurements were ∼1 mm in diameter.

In addition to being simple and predictable, the tuning method described above can provide fast tuning over large wavelength regions. The time that is needed for the signal (idler) frequency to stabilise after a temperature step is usually less than a minute, which is shown in Fig. 16. With small to modest OPO power levels the long-term mode-hop-free operation can be readily obtained after this. At high power levels, at about 2–2.5 times the threshold, there are occasional mode hops and multiple modes still few minutes after the temperature step. In particular this is the case when the OPO is operated at regions where the crystal losses are increased. An example of this is shown in the inset of Fig. 15. After the crystal temperature has stabilised, the pump laser can be scanned. In order to take the full advantage of the fast temperature scanning method, a pump laser with fast mode-hop-free tuning [7, 10] should be used. In our present system the tuning speed is limited by the pump laser. The pump laser is scanned by adjusting its temperature, which makes the scanning inherently slow. In practise, the scanning speed was limited to approximately 10 GHz/min. If the scanning speed was increased above this, the laser temperature could not follow the scan signal anymore, which led to instabilities in the pump laser. Such instabilities caused occasional OPO-cavity mode hops and tendency for weak side modes to arise. The slow tuning rate of the pump laser also leads to a dead time at the end of each scanning cycle because the pump frequency has to be restored to its initial value before a new scan can be started.

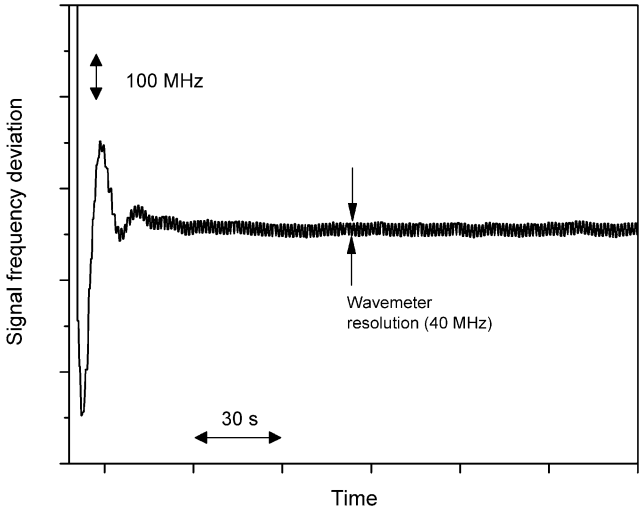

Fig. 16 Stabilisation of the OPO frequency after inducing a 1 K step to the crystal temperature. The time required for the frequency to stabilise is equal to the stabilisation time of the crystal temperature

5 Conclusion

In this paper we have experimentally studied thermal effects in a CW singly resonant optical parametric oscillator that provides watt-level idler output power in the 3-μm mid-infrared band. Thermal effects arise from the small optical absorption in the nonlinear crystal (MgO:PPLN) used for optical parametric conversion. We have limited our study to a regime in which thermal effects are dominated by the absorption of large signal power resonating in the OPO cavity. In this regime, the effects of pump and idler absorption are negligible.

We have reported an observation of optical bi-stability in a SRO that resonates the signal wavelength. The bi-stability is explained by a combined effect of thermal lensing and axial mismatch of the pump and signal beams. We have also studied the OPO spectral purity as a function on absorbed power and experimentally found that crystal heating caused by the absorption should be limited to below ∼1 K in order to avoid oscillation in multiple longitudinal modes. We have shown that, even if the intra-cavity signal power was limited by using a partly transmitting output coupler, the SRO is affected by a self-locking effect, which we believe to be of thermal origin. The effect of thermal locking is enhanced by residual modulation of the parametric gain curve, caused by frequency dependent losses in the OPO.

Finally, we have shown that, by careful thermal control of the SRO crystal, it is possible to attain very good long-term frequency and power stability without using an intra-cavity etalon or without actively stabilising the OPO to an external reference. We have also demonstrated that, without an etalon, it is possible to continuously tune the SRO frequency over several THz by simply combining the crystal temperature tuning with tuning of the pump laser that can provide a mode-hop-free tuning range of 140 GHz.

Acknowledgements The financial support of the Academy of Finland is gratefully acknowledged. University of Helsinki is acknowledged for funding the laboratory equipment needed in this work.

References

1. K.R. Lykke, P.-S. Shaw, L.M. Hanssen, G.P. Eppeldauer, Metrologia **36**, 141 (1999)
2. A.K.Y. Ngai, S.T. Persijn, I.D. Lindsay, A.A. Kosterev, P. Groß, C.J. Lee, S.M. Cristescu, F.K. Tittel, K.-J. Boller, F.J.M. Harren, Appl. Phys. B **89**, 123 (2007)
3. A.K.Y. Ngai, S.T. Persijn, G. von Basum, F.J.M. Harren, Appl. Phys. B **85**, 173 (2006) and several other articles in the Appl. Phys. B Special Issue: "Optics: Trends in Laser Sources, Spectroscopic Techniques and Their Applications to Trace-Gas-Detection"
4. E.V. Kovalchuk, D. Dekorsy, A.I. Lvovsky, C. Braxmaier, J. Mlynek, A. Peters, S. Schiller, Opt. Lett. **26**, 1430 (2001)
5. E.V. Kovalchuk, T. Schuldt, A. Peters, Opt. Lett. **30**, 3141 (2005)
6. W.R. Bosenberg, A. Drobshoff, J.I. Alexander, L.E. Myers, R.L. Byer, Opt. Lett. **21**, 1336 (1996)
7. A. Henderson, R. Stafford, Opt. Express **14**, 767 (2006)
8. S.E. Bisson, K.M. Armstrong, T.J. Kulp, M. Hartings, Appl. Opt. **40**, 6049 (2001)
9. G.K. Samanta, M. Ebrahim-Zadeh, Opt. Express **16**, 6883 (2008)
10. I. Lindsay, B. Adhimoolam, P. Groß, M. Klein, K. Boller, Opt. Express **13**, 1234 (2005)
11. M. Vainio, J. Peltola, S. Persijn, F.J.M. Harren, L. Halonen, Opt. Express **16**, 11141 (2008)
12. D.D. Lowenthal, IEEE J. Quantum Electron. **34**, 1356 (1998)
13. M.M.J.W. van Herpen, S.E. Bisson, F.J.M. Harren, Opt. Lett. **28**, 2497 (2003)
14. A. Henderson, R. Stafford, Appl. Phys. B **85**, 181 (2006)
15. L.E. Myers, W.R. Bosenberg, IEEE J. Quantum Electron. **33**, 1663 (1997)
16. S.T. Lin, Y.Y. Lin, Y.C. Huang, A.C. Chiang, J.T. Shy, Opt. Lett. **33**, 2338 (2008)
17. U. Straßner, J.-P. Meyn, R. Wallenstein, P. Urenski, A. Arie, G. Rosenman, J. Mlynek, S. Schiller, A. Peters, J. Opt. Soc. Am. B **19**, 1419 (2002)
18. M.M.J.W. van Herpen, Continuous-wave optical parametric oscillator for trace gas detection in life sciences, PhD thesis, Radboud University Nijmegen, 2004
19. E. Kovalchuk, Optical parametric oscillators for precision IR spectroscopy and metrology, Dissertation, Humboldt-Universität zu Berlin, 2007
20. A.J. Henderson, R. Stafford, P. Hoffman, *Laser Applications to Chemical, Security and Environmental Analysis, OSA Technical Digest (CD)* (Optical Society of America, 2008), paper LMC2
21. Y. Furukawa, K. Kitamura, A. Alexandrovski, R.K. Route, M.M. Fejer, G. Foulon, Appl. Phys. Lett. **78**, 1970 (2001)
22. L. Arizmendi, Phys. Status Solidi A **201**, 253 (2004)
23. G. Boyd, D. Kleinman, J. Appl. Phys. **39**, 3597 (1968)
24. S. Guha, F.J. Wu, J. Falk, IEEE J. Quantum Electron. **18**, 907 (1982)
25. D.R. Hall, P.E. Jackson, *The Physics and Technology of Laser Resonators* (Taylor & Francis, New York, 1989)
26. H. Abitan, T. Skettrup, J. Opt. A: Pure Appl. Opt. **7**, 7 (2005)
27. A.V. Smith, SNLO software, 4.0 edn. (2005)
28. A. Douillet, J.-J. Zondy, A. Yelisseyev, S. Lobanov, L. Isaenko, J. Opt. Soc. Am. B **16**, 1481 (1999)

29. A. Sennaroglu, A. Askar, F.M. Atay, J. Opt. Soc. Am. B **14**, 356 (1997)
30. M.E. Innocenzi, H.T. Yura, C.L. Fincher, R.A. Fields, Appl. Phys. Lett. **56**, 1831 (1990)
31. HC-Photonics, Taiwan, personal communication
32. T. Andres, P. Haag, S. Zelt, J.-P. Meyn, A. Borsutzky, R. Beigang, R. Wallenstein, Appl. Phys. B **76**, 241 (2003)
33. J.K. Yamamoto, K. Kitamura, N. Iyi, S. Kimura, Y. Furukawa, M. Sato, Appl. Phys. Lett. **61**, 2156 (1992)
34. R.O. Moore, G. Biondini, W.L. Kath, J. Opt. Soc. Am. B **19**, 802 (2002)
35. N.P. Barnes, J.A. Williams-Byrd, J. Opt. Soc. Am. B **12**, 124 (1995)
36. H.Y. Shen, H. Xu, Z.D. Zeng, W.X. Lin, R.F. Wu, G.F. Xu, Appl. Opt. **31**, 6695 (1992)
37. C. Richy, K.I. Petsas, E. Giacobino, C. Fabre, L. Lugiato, J. Opt. Soc. Am. B **12**, 456 (1995)
38. I. Breunig, J. Kiessling, B. Knabe, R. Sowade, K. Buse, Opt. Express **16**, 5662 (2008)
39. E.S. Polzik, H.J. Kimble, Opt. Lett. **16**, 1400 (1991)
40. A. Henderson, R. Stafford, Opt. Lett. **32**, 1281 (2007)
41. A.V. Okishev, J.D. Zuegel, Opt. Express **16**, 11141 (2008)
42. D.J.M. Stothard, I.D. Lindsay, M.H. Dunn, Opt. Express **12**, 502 (2004)
43. D.K. Serkland, R.C. Eckardt, R.L. Byer, Opt. Lett. **19**, 1046 (1994)
44. P.L. Hansen, P. Buchhave, Opt. Lett. **22**, 1074 (1997)
45. T. Ikegami, S. Slyusarev, S.I. Ohshima, Opt. Commun. **184**, 13 (2000)
46. P. Dubé, L.-S. Ma, J. Ye, P. Jungner, J.L. Hall, J. Opt. Soc. Am. B **13**, 2041 (1996)